



# Comparative effects of oncogenic mutations G12C, G12V, G13D, and Q61H on local conformations and dynamics of K-Ras

Sezen Vatansever<sup>a,b</sup>, Burak Erman<sup>c,\*</sup>, Zeynep H. Gümüş<sup>a,b,\*</sup>

<sup>a</sup>Department of Genetics and Genomic Sciences, Icahn School of Medicine at Mount Sinai, New York, NY, United States

<sup>b</sup>Icahn Institute for Data Science and Genomic Technology, New York, NY, United States

<sup>c</sup>Department of Chemical and Biological Engineering, College of Engineering, Koç University, Istanbul, Turkey



## ARTICLE INFO

### Article history:

Received 31 August 2019

Received in revised form 5 March 2020

Accepted 4 April 2020

Available online 9 April 2020

### Keywords:

K-Ras

K-Ras mutant

Molecular dynamics

Local dynamics

## ABSTRACT

K-Ras is the most frequently mutated protein in human cancers. However, until very recently, its oncogenic mutants were viewed as undruggable. To develop inhibitors that directly target oncogenic K-Ras mutants, we need to understand both their mutant-specific and pan-mutant dynamics and conformations. Recently, we have investigated how the most frequently observed K-Ras mutation in cancer patients, G12D, changes its local dynamics and conformations (Vatansever et al., 2019). Here, we extend our analysis to study and compare the local effects of other frequently observed oncogenic mutations, G12C, G12V, G13D and Q61H. For this purpose, we have performed Molecular Dynamics (MD) simulations of each mutant when active (GTP-bound) and inactive (GDP-bound), analyzed their trajectories, and compared how each mutant changes local residue conformations, inter-protein distance distributions, local flexibility and residue pair correlated motions. Our results reveal that in the four active oncogenic mutants we have studied, the  $\alpha 2$  helix moves closer to the C-terminal of the  $\alpha 3$  helix. However, P-loop mutations cause  $\alpha 3$  helix to move away from Loop7, and only G12 mutations change the local conformational state populations of the protein. Furthermore, the motions of coupled residues are mutant-specific: G12 mutations lead to new negative correlations between residue motions, while Q61H destroys them. Overall, our findings on the local conformational states and protein dynamics of oncogenic K-Ras mutants can provide insights for both mutant-selective and pan-mutant targeted inhibition efforts.

© 2020 Published by Elsevier B.V. on behalf of Research Network of Computational and Structural Biotechnology. This is an open access article under the CC BY-NC-ND license (<http://creativecommons.org/licenses/by-nc-nd/4.0/>).

## 1. Introduction

K-Ras is a small GTPase that plays a crucial role in cellular signaling and promotes cellular proliferation, survival, growth and differentiation [2]. The protein controls signaling networks by functioning as a molecular switch that cycles between an inactive GDP-bound and an active GTP-bound state [3,4]. The balance between the two states is regulated by guanine nucleotide exchange factors (GEFs) that bind to inactive K-Ras (K-Ras-GDP) and stimulate the exchange of GDP with GTP. After GTP binding, K-Ras becomes active (K-Ras-GTP) and can bind and activate its downstream effector proteins, such as Raf kinase, phosphatidylinositol 3-kinase (PI3K), and Ral guanine nucleotide dissociation stimulator (RalGDS) [5–7]. To terminate the downstream signaling,

active K-Ras catalyzes GTP hydrolysis to return to its inactive state. The intrinsic GTPase activity of K-Ras-GTP can be enhanced by GTPase-activating protein (GAP) binding [8,9]. A complete GTPase reaction requires well-ordered conformations of the protein active site, which includes the P-loop (residues 10–17), switch I (SI, residues 25–40) and switch II (SII, residues 60–74) regions (Fig. 1).

Based on The Catalog of Somatic Mutations in Cancer (COSMIC), the most frequently observed oncogenic K-Ras mutations in cancer patients are at active site residues G12 (89%), G13 (9%) and Q61 (1%) [5,10]. These mutations impair both intrinsic and GAP-accelerated GTPase activity while increasing the nucleotide exchange activity, which disturbs the balance between active and inactive states [11,12]. Since mutant K-Ras-GTP cannot return back to its inactive form, it continuously triggers the downstream signaling networks that are ultimately related with oncogenic cellular growth [5,13–15]. However, blocking the continuous activity of oncogenic K-Ras with selective mutant or pan-mutant inhibition remains a formidable task [16,17].

\* Corresponding authors at: Department of Genetics and Genomic Sciences, Icahn School of Medicine at Mount Sinai, New York, NY, United States (Z.H. Gümüş).

E-mail addresses: [berman@ku.edu.tr](mailto:berman@ku.edu.tr) (B. Erman), [zeynep.gumus@mssm.edu](mailto:zeynep.gumus@mssm.edu) (Z.H. Gümüş).

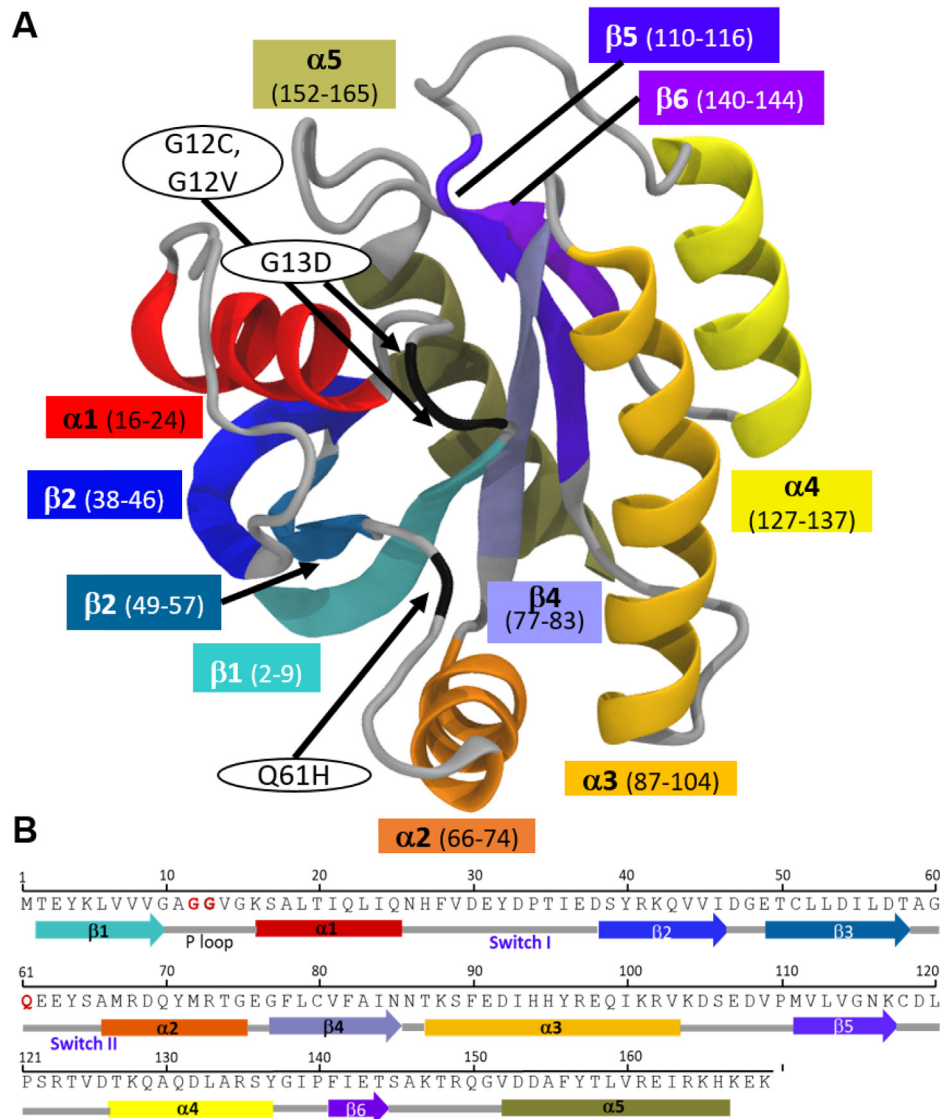


**Fig. 1.** K-Ras protein and the most frequently mutated residues. (A) Secondary structure of K-Ras in ribbon representation. Functional regions are in the same color as in K-Ras sequence. Arrows point to mutated residues. (B) Schematic of K-Ras sequence (residues 1–169). Arrows:  $\beta$ -sheets, rectangles:  $\alpha$ -helices.

Compelling evidence suggest that there are distinct mutation-specific effects on downstream effector signaling pathways [18]. Ihle et al. showed mutation-specific changes in downstream pathways in non-small cell lung cancer (NSCLC) cell lines [19]. Specifically, they observed that while both G12C and G12D mutations activate Ral signaling and decrease growth factor-dependent Akt activation, only G12D mutation activates phosphatidylinositol 3-kinase (PI-3-K) and mitogen-activated protein/extracellular signal-regulated kinase (MEK) signaling. In another study, Hammond *et al.* investigated the distinct effects of several KRAS mutations (G12V, G12D and G13D) on KRAS-mediated pathways by using quantitative analysis of the proteome of isogenic SW48 colon cancer cell lines [20]. They found that while G12 mutations induce the colon cancer stem cell marker DCLK1 and the receptor tyrosine kinase, the G13D mutation induces the tight-junction protein ZO-2. These studies suggest that K-Ras mutants can have distinct effects on downstream signaling pathways in cancer.

While distinct effects of different K-Ras mutations have been described in some studies, most studies so far have treated all K-Ras mutants as a single entity, considering the protein as either

wild-type or mutant [21]. To understand the conformational and dynamic changes due to the mutations, researchers have utilized molecular dynamics (MD) simulations and described the distinct global dynamics of mutant complexes (i.e., mutant K-Ras proteins in complex with GTP/GDP) [22,23]. However, identifying the unique local dynamics of K-Ras specific to its oncogenic mutation can also help understand the individual characteristics of each mutant protein, which can assist in the development of targeted therapies. In our previous work, we have presented a detailed study on the effects of the most recurrent oncogenic mutation, G12D, on local dynamic characteristics of both active and inactive K-Ras using long timescale MD simulations, and observed nucleotide-specific effects on local conformations and dynamics of the protein.

Following up on our previous study on the G12D mutant, here, we present mutation-specific (and agnostic) effects of other frequently observed oncogenic K-Ras mutants, including G12C, G12V, G13D and Q61H on local protein conformations and dynamics and provide an atomistic-level explanation for these effects. For this purpose, we have performed long timescale MD simulations of

each mutant in both GTP-bound active and GDP-bound inactive forms and compared them with each other and the wild-type protein. Briefly, we have first identified the individual effects of each mutation on local residue conformations by calculating the changes in intra-protein residue pair distances. Then, we have identified the favored conformations of residue pairs in each mutant protein complex by plotting the distributions of their distances. These provided information on how each oncogenic mutation alters the local conformational dynamics of active and inactive wild-type K-Ras. We next asked whether these oncogenic mutations caused certain protein regions to become more flexible or rigid. To understand and quantify mutation-specific local changes in protein flexibility, we compared the residue fluctuations of each mutant in both active and inactive form with those of wild-type K-Ras. Next, we aimed to understand the regulation of local protein dynamics by the allosteric coupling of residue fluctuations in each mutant system. For this purpose, we described the regulation of local protein motions by plotting the pair-wise correlations of residue fluctuations. Each mutant displayed distinct patterns in residue-residue correlation maps that revealed mutation-specific regulation of local dynamics. In summary, we have analyzed and compared the local dynamics of each oncogenic K-Ras mutant in both active and inactive forms with the wild-type protein, which revealed mutation-specific effects on local protein conformations and dynamics. We anticipate that our results will inform future studies on selective targeting of K-Ras oncogenic mutants in their active or inactive states.

## 2. Results

### 2.1. Conformational changes in k-ras due to oncogenic mutations G12C, G12V, G13D and Q61H

#### 2.1.1. In active K-Ras, residue G12 mutations cause SII to move away from both the $\alpha 3$ helix and the P-loop

To explore how oncogenic mutations alter the local residue conformations of K-Ras, we first performed MD simulations of the GTP- and GDP-bound oncogenic K-Ras mutants G12C, G12V, G13D and Q61H. Next, we analyzed each trajectory using a protocol from our previous study on G12D<sup>1</sup>, which we summarize in Methods. Briefly, for each GTP-bound protein, to understand the contribution of non-bonded residue-residue pairs to changes in local conformation [26,29], we defined a sphere with radius  $\sim 9.1$  Å around each residue, and calculated the time-averaged distance ( $\bar{R}_{ij}$ ) of all residues to the central residue within this sphere. Such a sphere around a residue includes both its contacting neighbors and non-bonded local interactions, and corresponds to its *second coordination shell*, as conceptualized within the popularly used protein dynamics analysis approach of Gaussian Network Modeling (GNM) [24–27] (see Methods). We then quantified the changes in residue-residue distances ( $\Delta\bar{R}_{ij}$ ) caused by each mutation by assuming K-Ras<sup>WT</sup> as the reference structure and used the first frame of its trajectory to determine the residue pairs (*ij*) within the second coordination shell. In Fig. 2, we show the  $\Delta\bar{R}_{ij}$  values for all residue pairs (*ij*), where positive values correspond to regions that move away from each other upon mutation and negative values correspond to regions that get closer. As suggested by the  $\Delta\bar{R}_{ij}$  values in Fig. 2A and C, the SII loop (Q61-E62) moves away from the  $\alpha 3$  helix (D92-H95) in G12 mutants G12C and G12V. Furthermore, SII residue Q61 also moves away from the P-loop (A11-G13).

MD simulations of the mutant K-Ras-GTP complexes revealed that similar to our observations in the G12D mutant in our earlier study [1], the salt bridge between E62 (SII) and K88 ( $\alpha 3$ ) in K-Ras<sup>WT</sup>-GTP disappears in other G12 mutants. Combined with our

observations in Fig. 2, these results suggest that SII moves away from its neighbors as a result of the disruption of the salt bridge between SII and  $\alpha 3$ . Intriguingly, in G13D mutant, the deviation of SII from its neighbors is not as remarkable as in G12 mutants.

In addition to the changes in SII distances, we also observed that the  $\alpha 3$  helix (Q99-K101) moves away from the Loop7 (E107) in G12C, G12V and G13D mutants (but not Q61H), as shown in Fig. 2.

#### 2.1.2. In active K-Ras, studied oncogenic mutations cause the P-loop, SI, SII and $\alpha 3$ regions to move away from their neighbors

In addition to analyzing the mutation effects on pairwise distances ( $\Delta\bar{R}_{ij}$ ), we also quantified the effects on individual conformations of residues relative to their neighbors'. Specifically, for each oncogenic mutant, we separately plot the average pairwise distance of each residue,  $\langle\Delta\bar{R}_i\rangle$ , as shown in Fig. 2. These plots revealed that in all oncogenic K-Ras mutants, the P-loop, SI, SII and the  $\alpha 3$  helix regions become distant from their neighbors, with the effect most pronounced in G12C and G13D mutants. However, the G12V mutant exhibits large deviations in both P-loop and SII, while the Q61H mutant shows distinctly strong deviations in SII.

In summary, based on our time-averaged inter-residue distance analysis, oncogenic mutations studied cause largest local conformational changes in the SII,  $\alpha 3$  and P-loop regions (Fig. 2). These analyses provide static information on mutational effects on local conformations. Next, to gain dynamic information, we investigated how the local conformations distributed over the simulation time, as described below.

#### 2.1.3. Oncogenic mutations at residue G12 alter the balance of residue pair distances between SII and $\alpha 3$ helix

To better understand the dynamic effects of mutations on local residue conformations in the regions that show the largest static deviations from the wild-type, we plot the distance distributions between C $\alpha$ -C $\alpha$  atoms of residue pairs in these regions for each mutant protein in both active and inactive form (Figs. 3–5). For a given residue pair, these distribution plots reveal whether the residue pair exhibits: (i) similar conformations in both wild-type and mutant protein simulations, leading to overlapping distribution patterns; or (ii) different conformations in the mutant than in the wild-type, leading to dissimilar distribution patterns. In addition, multiple peaks suggest that the residue pair obtains multiple conformations during the simulation, while a single peak suggests that the residue pair gets stuck in a single conformation.

From these plots, we observed that the distance distribution patterns exhibit distinct characteristics in each mutant system, suggesting that the oncogenic mutations we studied change the balance of distances between protein regions. Specifically, in *active K-Ras*<sup>WT</sup>, the distance distribution plots of SII loop- $\alpha 3$  region show only two peaks with narrow distributions (Figs. 3A-B, S1A-B). The first peak is at  $\sim 8.5$  Å for Q61-92 (8 Å for 62-92) and the second peak is at  $\sim 16.5$  Å for Q61-92 ( $\sim 13$  Å for 62-92), suggesting both close and distant conformations of the residue pairs, respectively. However, both C and V mutations at G12 decrease the number of conformations, leading to distribution curves with only a single peak at  $\sim 16.5$  Å for Q61-92 ( $\sim 13$  Å for 62-92) (Figs. 3A-B and S1A-B). These results suggest that after both G12C and G12V mutations, the residue pairs in the SII loop- $\alpha 3$  region populate at the distant conformation, which is consistent with the same population shift we observed after G12D mutation in our earlier study [1].

In *inactive K-Ras*, while the distances in the SII loop- $\alpha 3$  region were more widely spread, with peaks at larger distances in the wild-type inactive protein (Fig. 3C-D), the peaks correspond to shorter distances in G12C mutant (Figs. 3C, S1C). These results suggest that in inactive K-Ras, the SII loop- $\alpha 3$  region exhibits various conformations in wild-type but assumes a closer conformation

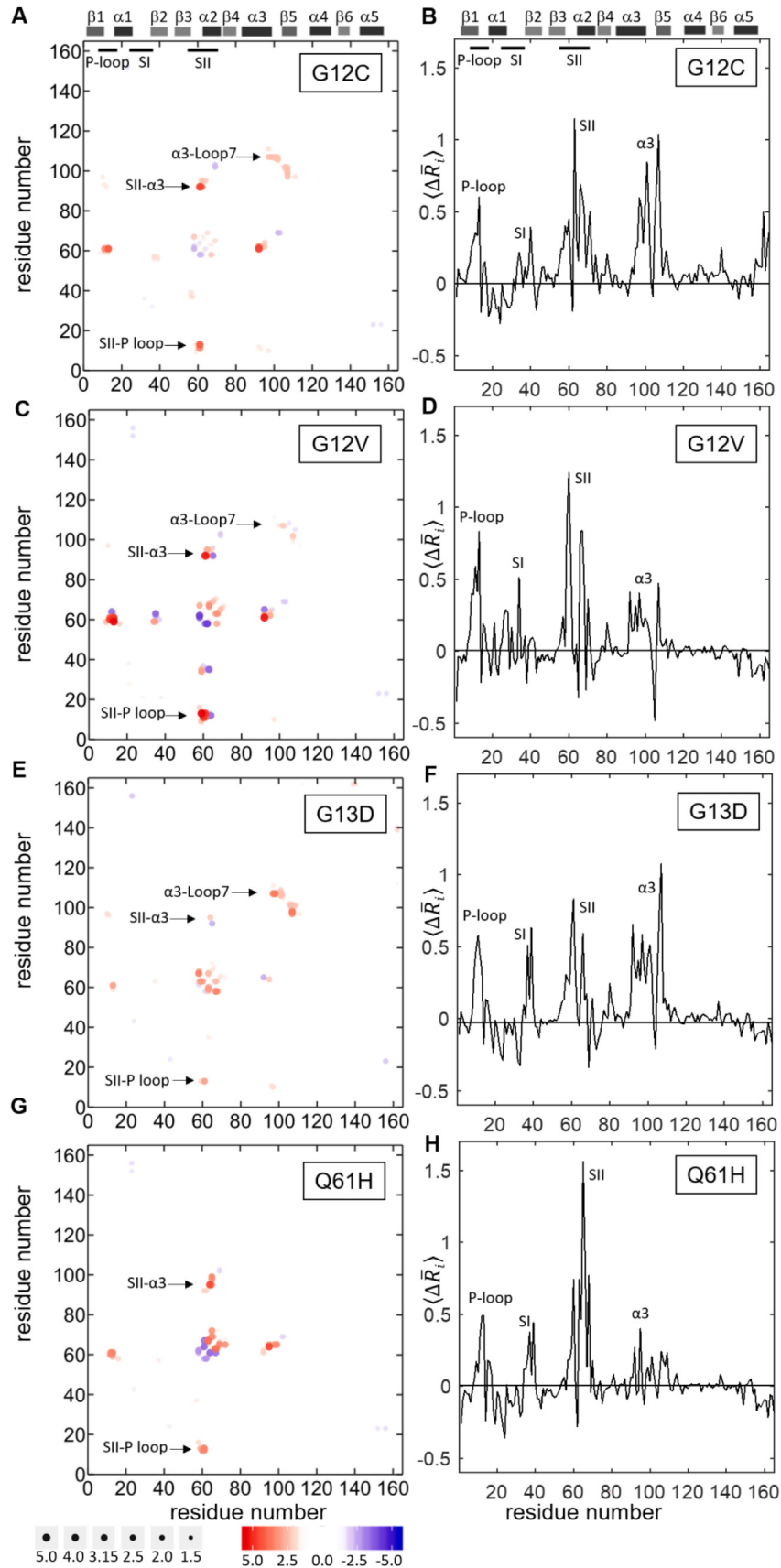


**Fig. 2.** Alterations in active K-Ras conformations due to oncogenic mutations. Left panels: changes in pairwise residue distances ( $\Delta R_{ij}$ ) in active K-Ras due to mutation. Positive  $\Delta R_{ij}$  values indicate divergent pairs (red); negative  $\Delta R_{ij}$  values indicate convergent pairs (blue). Right panels: all  $\Delta R_{ij}$  values averaged for each residue,  $\langle \Delta \bar{R}_i \rangle$ . Positive values indicate that the mutation causes a residue to move away from its neighbors; negative values indicate that a residue moves close to its neighbors. The predominant behavior for all studied mutants is positive (A-B) K-Ras<sup>G12C</sup> (C-D) K-Ras<sup>G12V</sup> (E-F) K-Ras<sup>G13D</sup> (G-H) K-Ras<sup>Q61H</sup>. (For interpretation of the references to color in this figure legend, the reader is referred to the web version of this article.)

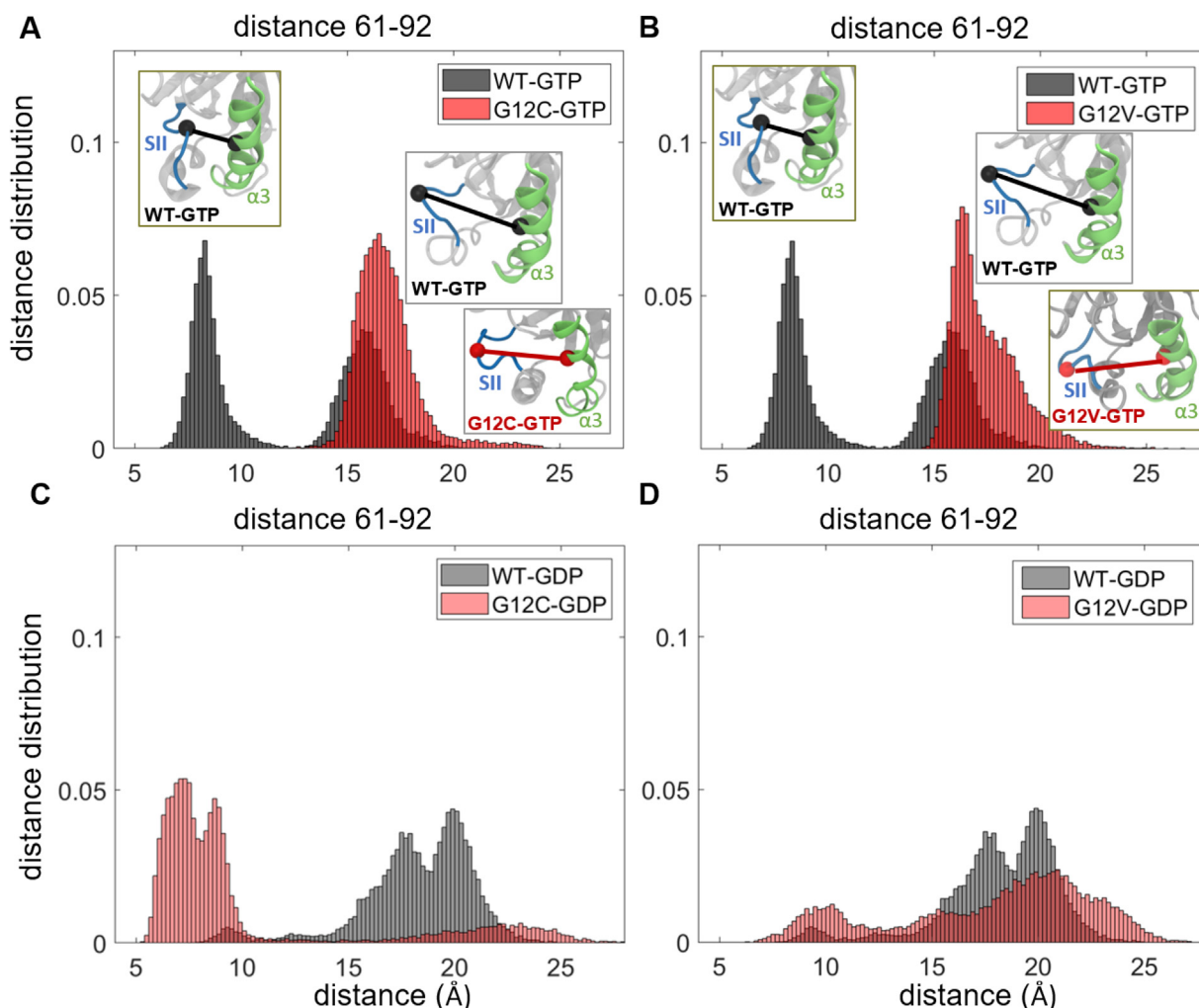


**Fig 3.** Distribution of distances  $W(R_{ij})$  between  $\alpha$ - $\alpha$  atoms of residue pairs in SII- $\alpha$ 3 region in wild-type and G12 mutant K-Ras proteins. GTP-bound active K-Ras (black: WT, red: mutant) (A) Q61-D92 in WT and G12C, (B) Q61-D92 in WT and G12V; GDP-bound active K-Ras (grey: WT, pink: mutant) (C) Q61-D92 in WT and G12C, (D) Q61-D92 in WT and G12V. (For interpretation of the references to color in this figure legend, the reader is referred to the web version of this article.)

after the G12C mutation, which is similar to that of the G12D mutation [1]. However, G12V mutation does not have such an effect, as shown in Figs. 3D and S1C.

#### 2.1.4. In both active and inactive K-Ras, mutations on P-loop and SII alter their conformational populations

In inactive K-Ras<sup>WT</sup>, the residue pair distances between the P-loop residues (A11-G13) and SII residues (Q61-E63) exhibit multimodal distributions related to multiple conformations of this region. However, the distance distribution plots (Figs. 4, S2-3) show that the mutations at the P-loop (G12C, G12D and G13D) and SII (Q61H) decrease the number of conformations of this region in inactive protein.

In contrast to the widely dispersed distances in inactive form, active K-Ras<sup>WT</sup> P-loop-SII distances show bimodal behavior with narrow ranges, which suggest two distinct conformations. While the P-loop-SII region can switch between the close and distant conformations in active K-Ras<sup>WT</sup>, in all active studied mutations it populates distant residue pair conformations within a wider range, including P-loop mutations at G12C (Fig. 4A-C), G12V (Fig S2A-B), G13D (Fig S2C) as well as at Q61H (Fig S3). We have observed the same distribution pattern in K-Ras<sup>G12D</sup> in our previous work [1].

#### 2.1.5. In active K-Ras, mutations at P-loop cause $\alpha$ 3 helix to move away from its neighbor, Loop7

In inactive K-Ras, the distances between  $\alpha$ 3 and Loop7 residues exhibit broad distributions, with two peaks in K-Ras<sup>WT</sup> and one peak in mutant proteins K-Ras<sup>G12C</sup>, K-Ras<sup>G12V</sup> and K-Ras<sup>G13D</sup> (Figs. 5, S4). However, upon activation, while these residue pair distances become less variable in K-Ras<sup>WT</sup> with narrow distribution curves, they become more distant and variable in the mutants with multiple-peak distance distribution curves (Figs. 4, S4).

#### 2.1.6. In active K-Ras, the G12C mutation causes the conformations of SII loop residues to become similar to those of inactive K-Ras<sup>WT</sup>

Distance distribution curves of the two residue pairs within the SII loop, T58-Q61 and Q61-64, show the same characteristics in both K-Ras<sup>WT</sup>-GDP (Fig S5C-D) and K-Ras<sup>G12C</sup>-GTP (Fig S5A-B). These curves have multiple peaks within the range of ~5–10 Å that are related to multiple conformations of this region in K-Ras<sup>WT</sup>-GDP and K-Ras<sup>G12C</sup>-GTP. However, their single-peak narrow distribution curves in K-Ras<sup>WT</sup>-GTP implies the invariable conformation of the residue pairs in SII.

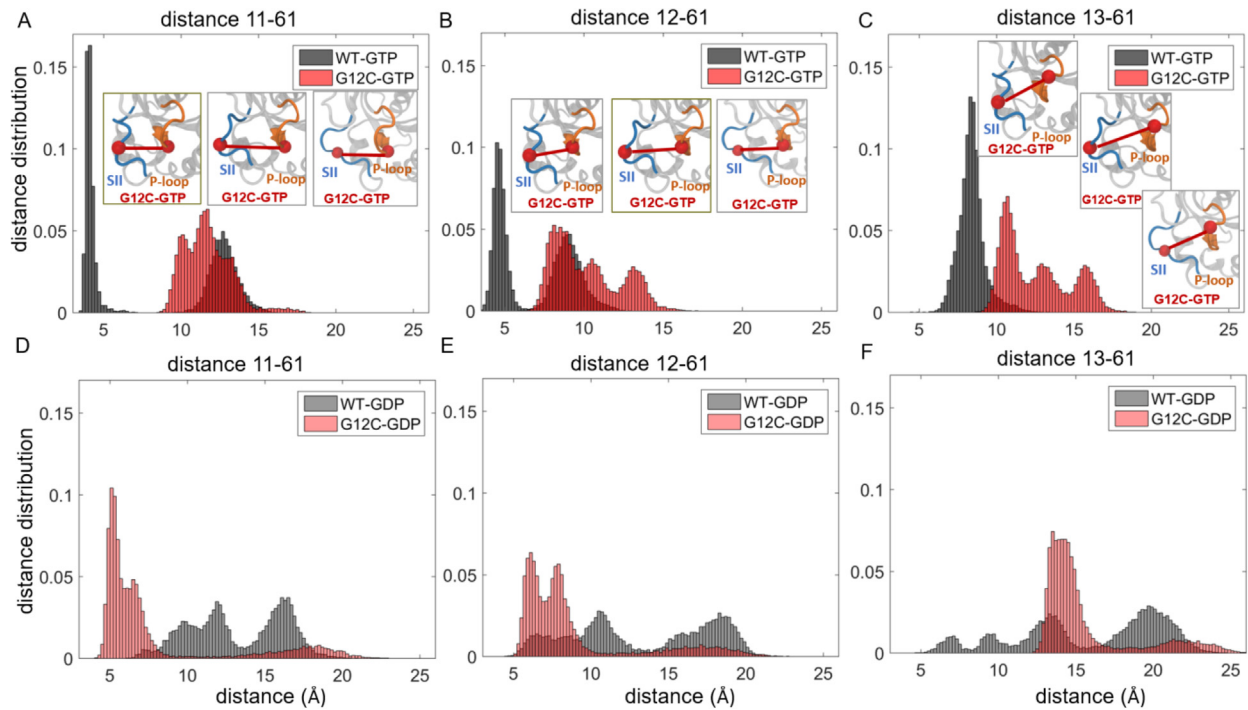


**Fig. 4.** Distribution of distances  $W(R_{ij})$  between C $\alpha$ -C $\alpha$  atoms of residue pairs in the P loop-SII region. GTP-bound active K-Ras (black: WT, red: G12C mutant) (A) A11-Q61, (B) G12D-Q61, (C) G12D-Q61; GTP-bound active K-Ras (grey: WT, pink: G12C mutant) (D) A11-Q61, (E) G12D-Q61, (F) G12D-Q61. (For interpretation of the references to color in this figure legend, the reader is referred to the web version of this article.)

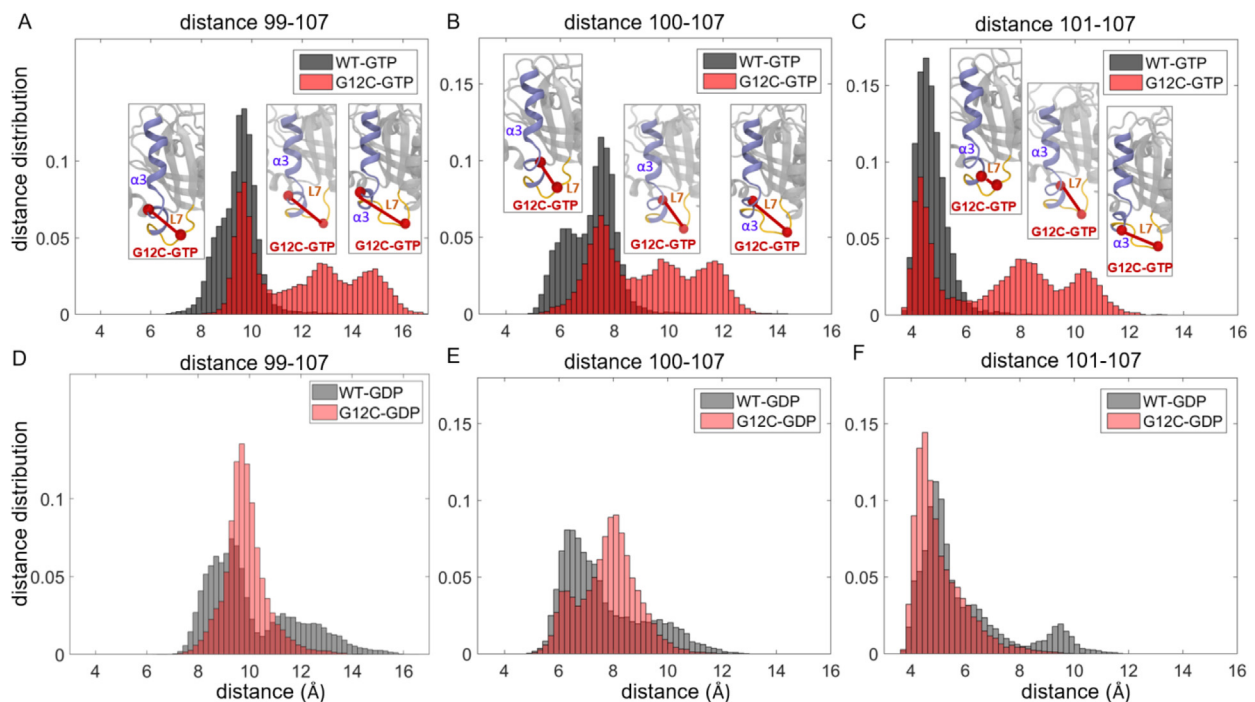


**Fig. 5.** Distribution of distances  $W(R_{ij})$  between C $\alpha$ -C $\alpha$  atoms of residue pairs in the  $\alpha$ 3-Loop7 region. GTP-bound active K-Ras (black: WT, red: G12C mutant) (A) A11-Q61, (B) G12D-Q61, (C) G12D-Q61; GTP-bound active K-Ras (grey: WT, pink: G12C mutant) (D) A11-Q61, (E) G12D-Q61, (F) G12D-Q61. (For interpretation of the references to color in this figure legend, the reader is referred to the web version of this article.)

### 2.1.7. In active K-Ras, all oncogenic mutations studied cause $\alpha$ 1 and $\alpha$ 5 helices to get stuck in their close conformation

In addition to the residue pairs above that move away from each other upon mutations as described above, we also observed regions that move towards each other, as shown in  $\Delta\bar{R}_{ij}$  maps in

Fig S6. Specifically, the negative  $\Delta\bar{R}_{ij}$  values indicate that the  $\alpha$ 1 and  $\alpha$ 5 helices get closer for all studied mutants of active K-Ras. Furthermore, their distance distribution curves each have a single peak (Fig S6A-D), indicating that the close conformation of the  $\alpha$ 1- $\alpha$ 5 region becomes dominant upon mutations. In contrast, in

wild-type protein, the two-peaked distance distribution curves of residue pairs (Fig S6A-D) suggests that they can obtain either a close or distant conformation. However, for inactive K-Ras, we did not observe such a conformational shift between the wild-type and mutant proteins (Fig S6E-H).

### 2.1.8. In active K-Ras, all oncogenic mutations studied cause $\alpha 2$ helix of SII to move towards C-terminal of the $\alpha 3$ helix

In the inactive protein, the distances between D69 ( $\alpha 2$ , SII) and R102-V103 ( $\alpha 3$ ) vary in the same range in both wild-type and mutant forms (Fig S7E-H). Conversely, in the active protein, the range of the distance values are not the same between the wild-type and mutant forms (Fig S7A-D). As evident from the distance distribution plots of the active K-Ras, D69 ( $\alpha 2$ , SII) and R102-V103 ( $\alpha 3$ ) become closer in K-Ras<sup>G12C</sup> followed by K-Ras<sup>G12V</sup>, K-Ras<sup>Q61H</sup>, K-Ras<sup>G12D</sup> and K-Ras<sup>G13D</sup>.

## 2.2. Dynamic changes in k-ras due to oncogenic mutations

### 2.2.1. In active K-Ras, oncogenic mutations on the P-loop increase the flexibility of SII region

Comparing the fluctuation amplitudes of residues in active wild-type versus mutant K-Ras, we show that SI, Loop $\beta 2-\beta 3$ , SII and  $\alpha 3$ -Loop7 regions are the flexible protein parts in all the P-loop mutant complexes G12C, G12V and G13D (Fig. 6A-C). Moreover, we observed that the salt bridge between E63 (SII) and R68 (SII) in the active K-Ras<sup>WT</sup> does not exist in the active P-loop mutants. In the absence of that bond, the flexibility of SII increases upon mutations in the P-loop and this region becomes the most fluctuating part of the mutant proteins (Fig. 6A-C).

### 2.2.2. In inactive K-Ras, G12C and G12V mutations do not affect the residue fluctuations

We compared the residue fluctuations of K-Ras<sup>WT</sup>-GDP with those of mutant K-Ras-GDP (Fig. 6E-H). Root mean square fluctuation (RMSF) plots of K-Ras<sup>G12C</sup>-GDP and K-Ras<sup>G12V</sup>-GDP show that they have similar fluctuations to those of wild-type. Specifically, SI, SII and  $\alpha 3$ -Loop7 regions are the most flexible parts in both wild-type and mutant inactive proteins. Therefore, we conclude that G12C and G12V mutations do not change the flexibility of the inactive K-Ras.

### 2.2.3. In inactive K-Ras, G13D mutation decreases the flexibility of SII (Fig. 6G)

Comparison of RMSF plots of the inactive K-Ras complexes shows that SII residues fluctuate less in K-Ras<sup>G13D</sup>-GDP than in K-Ras<sup>WT</sup>-GDP. This indicates that the SII region of the GDP-bound K-Ras becomes less flexible due to the G13D mutations.

### 2.2.4. The Q61 mutation alters protein flexibility differently than P-loop mutations (Fig. 6D, H)

Although oncogenic mutations on P-loop increase SII fluctuations, the Q61H mutation on SII does not affect SII fluctuations in active K-Ras. Interestingly, Q61H mutation slightly decreases the fluctuations of other protein parts, indicating the rigid nature of K-Ras<sup>Q61H</sup>-GTP. Specifically, we observed that there is a salt bridge between residues E62 (SII) and K16 ( $\alpha 1$ ). As a result of this bond, the amplitude of SII fluctuations in K-Ras<sup>Q61H</sup>-GTP are similar to those in K-Ras<sup>WT</sup>-GTP. However, Q61H mutation affects the flexibility of inactive protein in an opposite way. Most parts of the inactive protein become more flexible due to the Q61H mutation as indicated by the slightly higher RMSF fluctuation values in K-Ras<sup>Q61H</sup>-GDP.

## 2.3. Correlated residue pair motions in k-ras dynamics

### 2.3.1. Oncogenic K-Ras mutations do not disrupt correlated fluctuations of the residue pairs within the central $\beta$ -sheet

In previous work, we have observed that the residue pair correlation maps of active (GTP-bound) and inactive (GDP-bound) K-Ras<sup>WT</sup> show that fluctuations of the residues at the center of a six-stranded  $\beta$ -sheet are positively correlated (For details, see Vatansever et al [1]). Here, in residue pair correlation maps of the mutant proteins, we observe similar positive correlation patterns between the  $\beta$ -strand residues (Figs. 7 and 8). Therefore, oncogenic mutations of K-Ras do not appear to affect the coupling of  $\beta$ -strand fluctuations.

### 2.3.2. Oncogenic mutations at residue G12 alter negatively correlated motions in K-Ras

From the pairwise correlation analysis, we observed that the negative residue pair correlations of K-Ras are G12 mutation-specific, as shown in Fig. 7. Specifically, in the active wild-type protein,  $\alpha 1$  and SI move in correlation with the  $\beta 2-\beta 3$  regions; but this

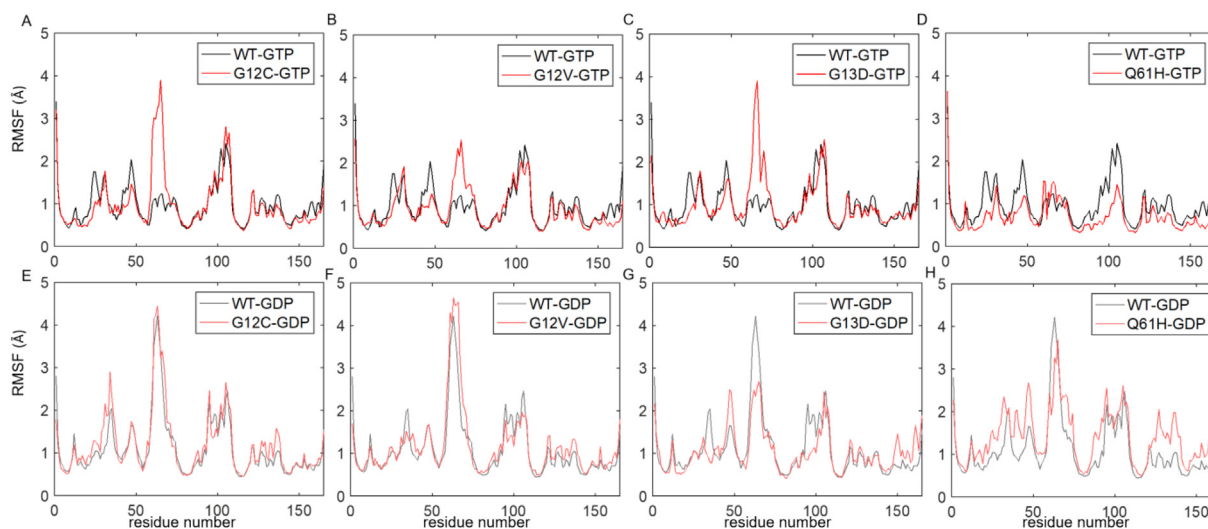


**Fig. 6.** Changes in K-Ras dynamics due to oncogenic mutations. Y-axis shows the RMSF values of residues. GTP-bound active K-Ras (black: WT, red: mutant) (A) G12C-GTP (B) G12V-GTP (C) G13D-GTP (D) Q61H-GTP; GDP-bound inactive K-Ras (grey: WT, pink: mutant) (E) G12C-GDP (F) G12V-GDP (G) G13D-GDP (H) Q61H-GDP. (For interpretation of the references to color in this figure legend, the reader is referred to the web version of this article.)

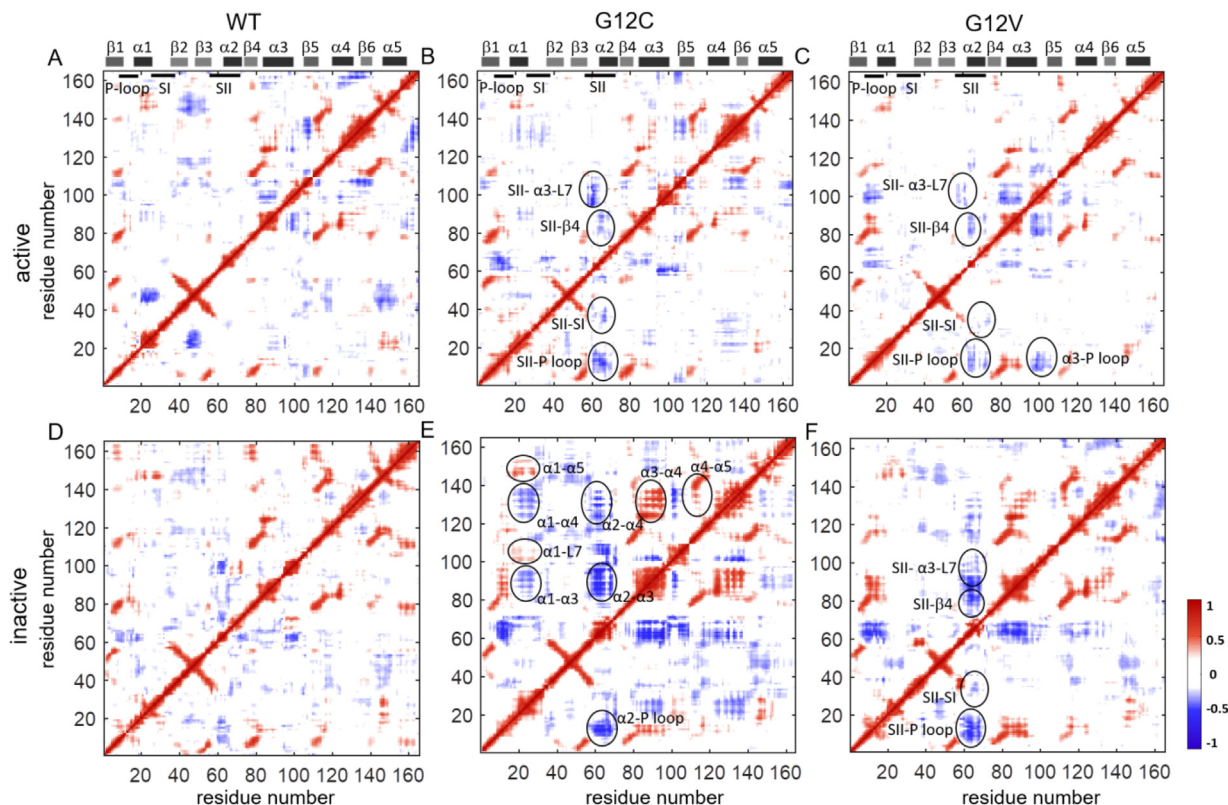


**Fig. 7.** Correlated motions of residue pairs in both active and inactive K-Ras G12 mutants. Positive correlations are in red and negative correlations are in blue. Pairwise correlation coefficients are plot for (A) K-Ras<sup>WT</sup>-GTP, (B) K-Ras<sup>G12C</sup>-GTP, (C) K-Ras<sup>G12V</sup>-GTP, (D) K-Ras<sup>WT</sup>-GDP, (E) K-Ras<sup>G12C</sup>-GDP, (F) K-Ras<sup>G12V</sup>-GDP. (For interpretation of the references to color in this figure legend, the reader is referred to the web version of this article.)

correlation is disturbed by the G12 mutations and new correlations occur. SII motions become strongly correlated with the P-loop, SI,  $\beta 4$  and  $\alpha 3$ -Loop7 regions upon G12C and G12V mutations. Additionally,  $\alpha 3$  motions become correlated with the guanine nucleotide binding sites due to G12V mutation. For the inactive states, correlations between the SII motions and the other protein regions increase in the G12C and G12V mutant.

### 2.3.3. In inactive K-Ras, G12C mutation significantly increases residue motion couplings

In the residue pair correlation analysis maps in Fig. 7, inactive G12C mutant map displays the most striking changes, where motions of the  $\alpha$ -helices become correlated with other protein regions (Fig. 7E). Specifically,  $\alpha 1$  motions are coupled to the Loop7 and  $\alpha 5$  motions while they are negatively correlated with  $\alpha 3$  and  $\alpha 4$ . Moreover,  $\alpha 2$  motions are negatively correlated with the P-loop,  $\alpha 3$  and  $\alpha 4$ . Furthermore,  $\alpha 4$  moves in correlation with  $\alpha 3$  and  $\alpha 5$ .

### 2.3.4. In active K-Ras, G13D mutation weakens the correlations of SII while causing new correlations for $\beta 2$ - $\beta 3$ loop (Fig. 8A, C)

SII motions in G13D mutant show similar, albeit much weaker correlation patterns with those in WT, G12C and G12D complexes. However,  $\beta 2$ - $\beta 3$  loop motions become negatively correlated with the central  $\beta$ -sheet ( $\beta 1$ -6) and positively correlated with SII. Additionally,  $\alpha 4$  region moves in correlation with  $\beta 1$ , the  $\beta 2$ - $\beta 3$  loop,  $\beta 4$ ,  $\alpha 3$ ,  $\beta 5$  and  $\alpha 5$ .

### 2.3.5. Q61H mutation destroys correlated motions in K-Ras dynamics

The negatively correlated residue pair motions in K-Ras completely disappear in active Q61H complex, as shown in Fig. 8B.

On the other hand, Q61H mutation causes correlated motions of  $\alpha 1$  the  $\beta 2$ - $\beta 3$  loop in the inactive protein (Fig. 8D).

## 3. Discussion

Oncogenic K-Ras mutants are high priority drug targets in cancer treatment. Hence, there have been considerable research efforts in directly targeting specific mutations or nucleotide-bound states (active or inactive) [30]. Recently, nucleotide-specific inhibitors of K-Ras<sup>G12C</sup> have shown promise [31], which have fueled further efforts towards directly targeting other K-Ras mutants in active or inactive states. Such selective targeting efforts have led to comparative analyses [32] that have improved our understanding of the mutation-specific effects at both clinical [33–35] and molecular level [19,36–39]. For atomistic level comparative analyses, studies have utilized MD simulations to focus on the differences in the global dynamics of active and/or inactive K-Ras mutants [22,23]. However, how different oncogenic mutations alter the *local* dynamics of K-Ras remains elusive. To address this question, in our previous work, we have studied the mechanisms by which oncogenic G12D mutation alters wild-type K-Ras conformations and dynamics and observed that it leads to changes specific to the bound nucleotide (GTP or GDP). Here, we build upon our previous study to understand whether the changes in nucleotide-bound K-Ras conformations and dynamics also show mutant-specific behavior. For this purpose, we investigated the changes in the conformational and dynamic behavior of active and inactive K-Ras caused by its most frequently observed oncogenic mutants other than G12D, which are G12C, G12V, G13D and Q61H. We analyzed the dynamics of each mutant protein in depth and compared them to those of the wild-type in both active and inactive forms. Our findings strongly suggest that the intrinsic

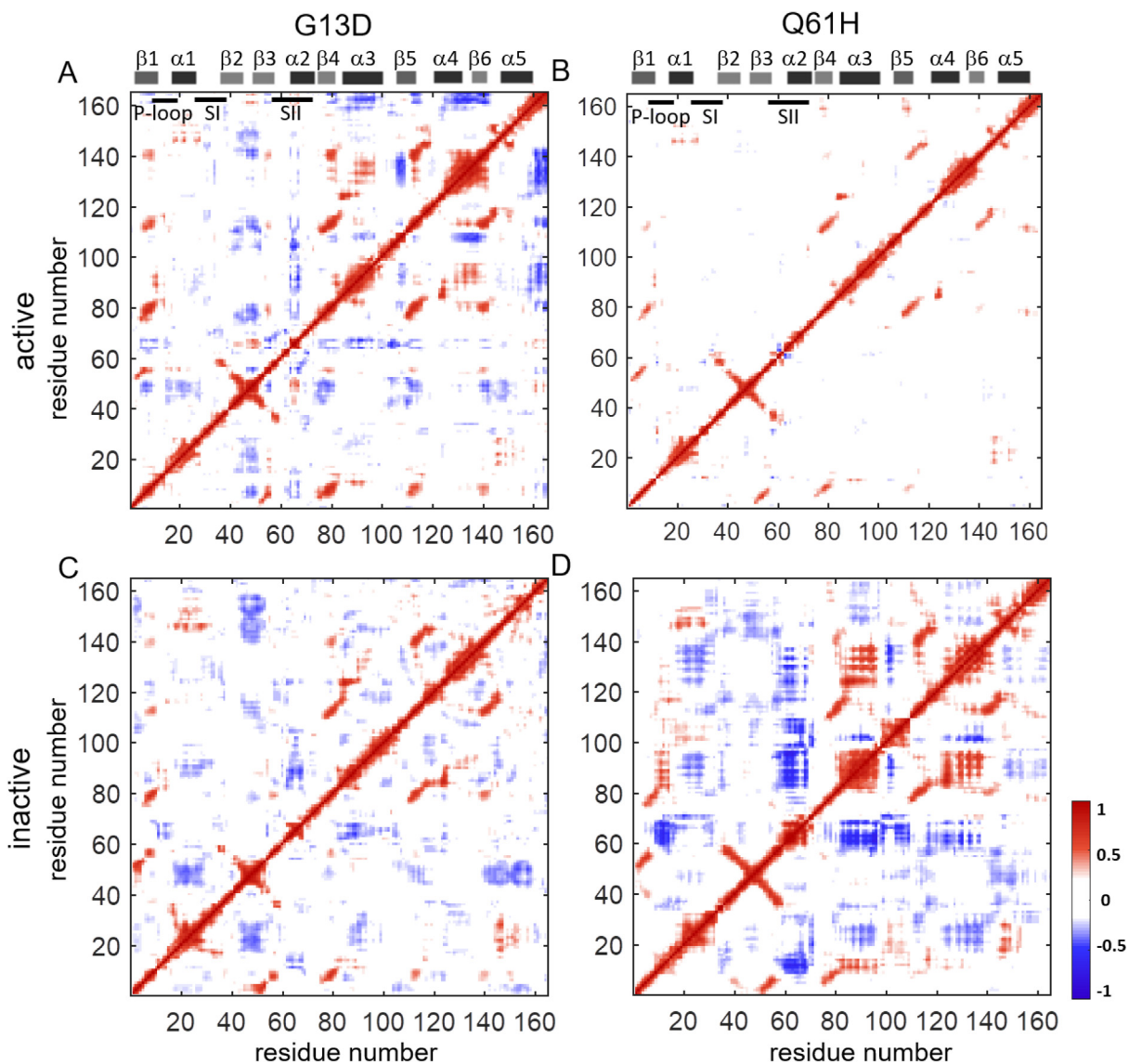


**Fig. 8.** Correlated motions of residue pairs in both active and inactive G13D and Q61H mutants. Positive correlations are in red and negative correlations are in blue. Pairwise correlation coefficients are plot for (A) K-Ras<sup>G13D</sup>-GTP, (B) K-Ras<sup>Q61H</sup>-GTP, (C) K-Ras<sup>G13D</sup>-GDP, (D) K-Ras<sup>Q61H</sup>-GDP. (For interpretation of the references to color in this figure legend, the reader is referred to the web version of this article.)

dynamic characteristics of the studied oncogenic K-Ras mutants are different than those of K-Ras<sup>WT</sup>. As other studies have also shown differences in K-Ras mutant oncoproteins in terms of transforming ability, GTP binding, anchorage-independent growth, and migration capacities [40], our findings on differences in local dynamics can help better understand the mechanisms that underlie such mutant-specific differences in K-Ras biology. Collecting such information on local residue conformations and their dynamic features is also a critical step towards the design of mutant specific and potent small targeting molecules [41]. In summary, knowledge we have generated on mutant-specific local changes can help better understand the mechanisms that underlie the biological differences between K-Ras mutants, and further inform targeted drug design.

To evaluate mutation-specific changes in K-Ras conformations, we have used residue pair distance calculations. Fig. 2 shows residue pair distance maps and Figs. 3–5 show their distance distributions, which reveal significantly increased distances caused by oncogenic mutations. As shown in Figs. 2–4, residues Q61-E62 (SII) move away from A11-G13 (P-loop) and D92(α3) in the active

G12 mutant complexes. We also observed changes in the protein structure, where the salt bridge between E62 (SII) and K88 (α3) in K-Ras<sup>WT</sup>-GTP disappears upon mutations. Our integrated structural and conformational analysis revealed that G12 mutations disturb this salt bridge between SII and α3, leading SII to move away from its neighbors. The importance of the connections within this SII-α3 region for the K-Ras dynamics was emphasized in previous studies [42]. First, it was shown that the interactions between SII and α3 (i.e. M67-Q99/I100, F78/C80-I100) is specific to K-Ras by comparing it with the other isoforms –N-Ras and H-Ras. Then, this SII-α3 region was defined as an “allosteric switch” in active K-Ras based on the observation of a shift in relative SII-α3 conformations [51]. Consistent with these studies, we identified specific effects of the studied oncogenic K-Ras mutations on structure and conformations of this region. Other studies have established that K-Ras mutations significantly reduce GAP-mediated GTP hydrolysis [39], where SII region is the GAP-binding site. Hence, mutational changes in SII conformations relative to those of other regions may potentially disrupt GAP binding and thereby GAP-assisted GTPase activity.

Our distance analysis further reveals that all studied oncogenic mutations cause  $\alpha 1$  and  $\alpha 5$  helices to get stuck in their close conformation in active K-Ras (K-Ras-GTP). Previous studies have emphasized the importance of the interaction of the  $\alpha 5$  helix with the lipidated hypervariable region (HVR) and membrane lipids for the K-Ras membrane orientation. These studies have used MD simulations with the HVR attached to the lipid membrane to understand the membrane orientation of the catalytic domain of an oncogenic K-Ras (i.e. K-Ras<sup>G12V</sup> [43,44]), but have not compared different mutant proteins or nucleotide states. Therefore, MD simulations of different membrane-bound oncogenic K-Ras proteins, as well as their comparative analyses are useful for further understanding the effects of oncogenic mutations on K-Ras dynamics.

To quantify how the studied oncogenic mutations change dynamic behavior of K-Ras, we used RMSF calculations, which showed higher fluctuation amplitudes for SII residues in active P-loop mutants as compared to wild-type (Fig. 6A-C). We further observed that this change in protein flexibility is associated with other structural changes, including the disappearance of a salt bridge within the SII region (i.e., E63-R68). However, unlike the P-loop mutants, Q61H mutation does not alter SII fluctuations (Fig. 7D), as another salt bridge forms between E62 (SII) and K16 ( $\alpha 1$ ) in the active protein. This salt bridge disappears in inactive K-Ras<sup>Q61H</sup>-GDP, leading to increased SII fluctuations (Fig. 5H). However, in terms of the flexibility of GDP-bound inactive protein complexes, only the G13D mutant differs from the wild-type. Notably, SII fluctuations only decrease in the G13D mutant, as depicted in the RMSF plot (Fig. 6G). This finding is consistent with experimental studies [39] that have shown that the GDP to GTP nucleotide exchange is similar for K-Ras<sup>WT</sup> and all its mutants, but is faster in the G13D mutant. While this may contribute to the more aggressive biology of tumors with G13D mutation [39], its combination with the decreased flexibility of the nucleotide-binding site SII may also provide a more accessible active site for small-molecules that bind to G13D mutant K-Ras.

We next investigated if and how the studied oncogenic mutations alter the fluctuations of correlated residue pairs, as these can be crucial in the regulation of protein dynamics, and thereby protein activity [45]. For this purpose, we calculated and compared the pairwise residue correlation coefficients of the mutant proteins, maps of which showed mutation-specific patterns (Figs. 7–8). Specifically, in active G12 mutants G12C and G12V, pairwise residue fluctuations in SII become negatively correlated, which we have previously also observed in G12D<sup>1</sup>. We next chose residues representative of the SII region in these two mutants (Q61 in K-Ras<sup>G12C</sup>-GTP and S65 in K-Ras<sup>G12V</sup>-GTP), and studied in detail their correlations with other protein parts (Fig S7A-B). In K-Ras<sup>G12C</sup>-GTP, Q61(SII) shows negative correlations with residues 96–105 ( $\alpha 3$ -Loop7) and 10–17 (P-loop). As we discovered in our distance calculations, in G12C mutants SII also becomes distant from the  $\alpha 3$ -Loop7 and P-loop regions. Similarly, in K-Ras<sup>G12V</sup>-GTP, S65 (SII) becomes negatively correlated with and distant from residues S89 ( $\alpha 3$ ) and 10–14 (P-loop). In summary, we have observed that in active K-Ras, G12 mutations cause SII to negatively correlate with and move away from  $\alpha 3$ -Loop7 and P-loop regions. Next, we studied the correlations of these residues in inactive K-Ras. We observed that in K-Ras<sup>G12C</sup>-GDP, Q61 (SII) shows strong negative correlations with C12 (P-loop) and H95 ( $\alpha 3$ ). The distance distribution plots show that SII and P-loop populate distant conformations compared to K-Ras<sup>WT</sup>-GTP, while SII- $\alpha 3$  regions become closer. On the other hand, in K-Ras<sup>G12V</sup>-GDP, Q61 (SII) shows negative correlations with and becomes distant from the P-loop and  $\alpha 3$ . In the K-Ras<sup>G13D</sup>-GTP complex, Y64 (SII) exhibits negative correlations with C-terminal of the  $\beta 3$  (Fig S7C) while it moves away from the same region (Fig. 2E). In active Q61H mutant,

G12 fluctuates in negative correlation with SII region (Fig S7F) and moves away from the SII residues (Fig S3).

Combining coefficient calculations with the RMSF values, we observed that SII fluctuations become negatively correlated with other residue pair fluctuations when their amplitudes increase due to the mutations. Specifically, SII fluctuations increase in K-Ras<sup>G12C</sup>-GTP, K-Ras<sup>G12V</sup>-GTP and K-Ras<sup>G13D</sup>-GTP (Fig. 6A-C) and become negatively correlated with the fluctuations of other residues (Figs. 7B-C, 8A). We also observed the opposite of that relation in the K-Ras<sup>Q61H</sup>-GTP dynamics. SII fluctuations do not increase after Q61H mutation and they do not become correlated with the other protein parts.

In summary, we defined the unique dynamic behavior of oncogenic K-Ras mutants most frequently observed in cancer patients by utilizing long-time scale MD simulations. Comparative analysis of simulation data revealed common and distinct mechanisms of how oncogenic mutations affect K-Ras local conformations and dynamics. Associating the structural, conformational and dynamic alterations in active and inactive mutant proteins, our results provide a holistic understanding of effects of the mutations on local dynamics of K-Ras proteins. Such an understanding of the oncogenic mutant-specific dynamic characteristics of K-Ras proteins can inform the development of new direct inhibitor small molecules that selectively bind to active or inactive mutant K-Ras proteins.

## 4. Methods

### 4.1. MD simulations

We performed all-atom MD simulations of K-Ras<sup>G12C</sup>, K-Ras<sup>G12V</sup>, K-Ras<sup>G13D</sup> and K-Ras<sup>Q61H</sup> proteins bound to Mg<sup>2+</sup>GTP or Mg<sup>2+</sup>GDP. For construction of initial structures, we followed the analysis steps in our previous study (For details see Supplementary) [1]. Using NAMD 2.10 [46] with AMBER ff99SB [47] and general amber force fields (GAFF) [48], we performed MD simulations of each mutant protein again following the steps from our previous study [49], details of which we present in Supplementary. We ran 1 microsecond MD simulations of each complex in replicate and analyzed the last 900 ns of each simulation. We recorded the atomic coordinates  $\hat{R}$  from the simulation trajectories in every 10 ps and aligned them to the first frame using VMD software 1.9.2 [50]. To identify salt bridge formations within the protein residues, we used Salt Bridges Plugin, Version 1.1, of VMD. We visualized the trajectories with VMD.

### 4.2. Residue pair distance calculations

We quantified the oncogenic mutation effects on residue pair distances using a computational approach described in our previous work [1]. In detail, based on the Gaussian network model (GNM) [24–27], we assumed the maximum C $\alpha$ -C $\alpha$  distance separation between two contacting residues as  $\sim 7.2$  Å [28], and thereby defined a volume  $V$  with a radius of  $r_1 \sim 7.2$  Å as the ‘first coordination shell’. In addition to the residue contacts within the ‘first coordination shell’, the contribution of non-bonded interactions to higher-order coordination shells can be important [29,26]. Therefore, we defined the ‘second coordination shell’ at twice the volume of the first, with a radius of  $\sim 9.1$  Å and included the residue pairs within their ‘second coordination shell’ in K-Ras structures in our residue pair distance analysis [26]. Briefly, we computed the C $\alpha$ -C $\alpha$  distances of residue pairs ( $i, j$ ) in wild-type K-Ras (the reference state) and in mutant K-Ras complexes (the final state) (For details see Supplementary). For every residue pair ( $i, j$ ) within the second coordination shell (radius of  $\sim 9.1$  Å) we calculated its

time-averaged distance in K-Ras<sup>WT</sup> ( $\bar{R}_{ij}^{WT}$ ), in mutant K-Ras ( $\bar{R}_{ij}^{MUT}$ ) and the difference ( $\Delta\bar{R}_{ij}$ ), where  $\Delta\bar{R}_{ij} = \bar{R}_{ij}^{MUT} - \bar{R}_{ij}^{WT}$ . The magnitude of the difference value is the degree of conformational change caused by the mutation. The left column of Fig. 1 presents residue pair distance maps in K-Ras mutants, where positive  $\Delta\bar{R}_{ij}$  values suggest that a residue  $i$  moves away from residue  $j$  and negative values suggest that the residues get closer.

To quantify the changes in local volumes due to the mutations, we calculated the average of all  $\Delta\bar{R}_{ij}$  values using the same approach in our previous study [1]. For all residues  $j$  in the second coordination shell of residue  $i$ , we computed averaged  $\Delta\bar{R}_{ij}$  values for each residue  $i$  based on the formula of  $\langle\Delta\bar{R}_i\rangle = \sum_j \Delta\bar{R}_{ij}/N_n$ , where  $N_n$  is the total number residues ( $j$ ) in the second coordination shell of residue  $i$  (For details see Fig S8). The resulting  $\langle\Delta\bar{R}_i\rangle$  values provide a scale for the change in volume around each residue ( $i$ ) upon mutation.

#### 4.3. Distance distributions between residue pairs

We first calculated the pairwise distance,  $R_{ij}$  for each residue pair ( $i, j$ ), and then the normalized distribution of these distances,  $W(R_{ij})$ , as we previously described [49]. Briefly, for every time point  $t$  of the MD simulation,  $R_{ij}(t)$  simply corresponds to  $\sqrt{(R_i(t) - R_j(t))^2}$ . Next, to calculate  $W(R_{ij})$ , we divided the range of  $R_{ij}(t)$  across the time course of the simulation, ( $\max\{R_{ij}(t_1), R_{ij}(t_2), \dots\} - \min\{R_{ij}(t_1), R_{ij}(t_2), \dots\}$ ), into small bins of width 0.2 and counted the number of observed distances in each bin using the Histogram function of the MATLAB tool from MathWorks (Natick, MA). For example, for  $W(R_{ij})$  values of residue pair (61, 92), see y-axes of Fig. 3.

#### 4.4. Residue pair correlation calculations

We calculated the correlation coefficients of residue pair fluctuations to identify those whose fluctuations were coupled during protein motions.  $C_{ij}$  is the correlation coefficient value of a residue pair ( $ij$ ) that varies from  $-1$  to  $1$ . For a perfectly positively correlated residue pair,  $C_{ij}$  equals to  $1$ , and to  $-1$  for a perfectly negatively correlated residue pair. However, it equals to  $0$  if the residue pair fluctuations are not correlated. We computed the  $C_{ij}$  values for every residue pair in each K-Ras mutant using the algorithm in our previous study [49].

#### CRedit authorship contribution statement

**Sezen Vatansever:** Conceptualization, Methodology, Software, Formal analysis, Investigation, Data curation, Writing - original draft, Visualization. **Burak Erman:** Conceptualization, Methodology, Investigation, Resources, Writing - review & editing, Supervision. **Zeynep H. Gümüş:** Conceptualization, Methodology, Investigation, Resources, Writing - review & editing, Supervision, Funding acquisition.

#### Acknowledgements

ZHG acknowledges funding from the LUNGEvity Foundation and start-up funds from the Department of Genetics and Genomics and the Icahn Institute for Data Science and Genomic Technology. We would also like to thank Dr. Myvizhi Esai Selvan for help with one of the figures.

#### Declarations of interest

None.

#### Appendix A. Supplementary data

Supplementary data to this article can be found online at <https://doi.org/10.1016/j.csbj.2020.04.003>.

#### References

- [1] Vatansever S, Erman B, Gümüş ZH. Oncogenic G12D mutation alters local conformations and dynamics of K-Ras. *Sci Rep* 2019;9:11730. <https://doi.org/10.1038/s41598-019-48029-z>.
- [2] Herrmann C, Nassar N. Ras and its effectors. *Prog Biophys Mol Biol* 1996;66:1–41.
- [3] Milburn MV et al. Molecular switch for signal transduction - structural differences between active and inactive forms of protooncogenic Ras proteins. *Science* 1990;247:939–45. <https://doi.org/10.1126/science.2406906>.
- [4] Vetter IR, Wittinghofer A. Signal transduction - the guanine nucleotide-binding switch in three dimensions. *Science* 2001;294:1299–304. <https://doi.org/10.1126/science.1062023>.
- [5] Lu S et al. Ras conformational ensembles, allostery, and signaling. *Chem Rev* 2016;116:6607–65. <https://doi.org/10.1021/acs.chemrev.5b00542>.
- [6] Fetis SK et al. Allosteric effects of the oncogenic RasQ61L mutant on Raf-RBD. *Structure* 2015;23:505–16. <https://doi.org/10.1016/j.str.2014.12.017>.
- [7] Sprang SR. G proteins, effectors and GAPs: structure and mechanism. *Curr Opin Struct Biol* 1997;7:849–56.
- [8] Glennon TM, Villa J, Warshel A. How does GAP catalyze the GTPase reaction of Ras?: A computer simulation study. *Biochemistry* 2000;39:9641–51. <https://doi.org/10.1021/bi000640e>.
- [9] Scheffzek K et al. The Ras-RasGAP complex: structural basis for GTPase activation and its loss in oncogenic Ras mutants. *Science* 1997;277:333–8. <https://doi.org/10.1126/science.277.5324.333>.
- [10] Prior IA, Lewis PD, Mattos C. A comprehensive survey of Ras mutations in cancer. *Cancer Res* 2012;72:2457–67. <https://doi.org/10.1158/0008-5472.CAN-11-2612>.
- [11] Bera AK et al. Structural basis of the atypical activation mechanism of KRAS (V14I). *J Biol Chem* 2019;294:13964–72. <https://doi.org/10.1074/jbc.RA119.009131>.
- [12] Hernandez-Porras I et al. K-RasV14I recapitulates Noonan syndrome in mice. *Proc Natl Acad Sci U S A* 2014;111:16395–400. <https://doi.org/10.1073/pnas.1418126111>.
- [13] Schubert S, Shannon K, Bollag G. Hyperactive Ras in developmental disorders and cancer. *Nat Rev Cancer* 2007;7:295–308. <https://doi.org/10.1038/nrc2109>.
- [14] Smith MJ, Neel BG, Ikura M. NMR-based functional profiling of RASopathies and oncogenic RAS mutations. *Proc Natl Acad Sci U S A* 2013;110:4574–9. <https://doi.org/10.1073/pnas.1218173110>.
- [15] Adjei AA. Blocking oncogenic Ras signaling for cancer therapy. *J Natl Cancer Inst* 2001;93:1062–74.
- [16] Ostrem JM, Shokat KM. Direct small-molecule inhibitors of KRAS: from structural insights to mechanism-based design. *Nat Rev Drug Discov* 2016. <https://doi.org/10.1038/nrd.2016.139>.
- [17] Marcus K, Mattos C. Direct attack on RAS: intramolecular communication and mutation-specific effects. *Clin Cancer Res* 2015;21:1810–8. <https://doi.org/10.1158/1078-0432.ccr-14-2148>.
- [18] Hobbs GA, Der CJ, Rossman KL. RAS isoforms and mutations in cancer at a glance. *J Cell Sci* 2016;129:1287–92. <https://doi.org/10.1242/jcs.182873>.
- [19] Ihle NT et al. Effect of KRAS oncogene substitutions on protein behavior: implications for signaling and clinical outcome. *J Natl Cancer Inst* 2012;104:228–39. <https://doi.org/10.1093/jnci/djr523>.
- [20] Hammond DE et al. Differential reprogramming of isogenic colorectal cancer cells by distinct activating KRAS mutations. *J Proteome Res* 2015;14:1535–46. <https://doi.org/10.1021/pr501191a>.
- [21] Miller MS, Miller LD. RAS mutations and oncogenesis: not all RAS mutations are created equally. *Front Genet* 2011;2:100. <https://doi.org/10.3389/fgene.2011.00100>.
- [22] Pantasar T et al. Assessment of mutation probabilities of KRAS G12 missense mutants and their long-timescale dynamics by atomistic molecular simulations and Markov state modeling. *PLoS Comput Biol* 2018;14. <https://doi.org/10.1371/journal.pcbi.1006458>.
- [23] Lu S, Jang H, Nussinov R, Zhang J. The Structural Basis Of Oncogenic Mutations G12, G13 and Q61 in small GTPase K-Ras4B. *Sci Rep* 2016;6:21949. <https://doi.org/10.1038/srep21949>.
- [24] Haliloglu T, Bahar I, Erman B. Gaussian dynamics of folded proteins. *Phys Rev Lett* 1997;79:3090–3. <https://doi.org/10.1103/PhysRevLett.79.3090>.
- [25] Bahar I, Atilgan AR, Demirel MC, Erman B. Vibrational dynamics of folded proteins: significance of slow and fast motions in relation to function and stability. *Phys Rev Lett* 1998;80:2733–6. <https://doi.org/10.1103/PhysRevLett.80.2733>.

- [26] Atilgan AR, Akan P, Baysal C. Small-world communication of residues and significance for protein dynamics. *Biophys J* 2004;86(1):85–91. [https://doi.org/10.1016/S0006-3495\(04\)74086-2](https://doi.org/10.1016/S0006-3495(04)74086-2).
- [27] Bahar I, Atilgan AR, Erman B. Direct evaluation of thermal fluctuations in proteins using a single-parameter harmonic potential. *Fold Des* 1997;2:173–81. [https://doi.org/10.1016/S1359-0278\(97\)00024-2](https://doi.org/10.1016/S1359-0278(97)00024-2).
- [28] Tuzmen C, Erman B. Identification of ligand binding sites of proteins using the Gaussian Network Model. *PLoS ONE* 2011;6. <https://doi.org/10.1371/journal.pone.0016474>.
- [29] Woodcock LV. Entropy difference between the face-centred cubic and hexagonal close-packed crystal structures. *Nature* 1997;385:141–3. <https://doi.org/10.1038/385141a0>.
- [30] O'Bryan JP. Pharmacological targeting of RAS: recent success with direct inhibitors. *Pharmacol Res* 2019;139:503–11. <https://doi.org/10.1016/j.phrs.2018.10.021>.
- [31] Ostrem JM, Peters U, Sos ML, Wells JA, Shokat KM. K-Ras(G12C) inhibitors allosterically control GTP affinity and effector interactions. *Nature* 2013;503:548–51. <https://doi.org/10.1038/nature12796>.
- [32] Ni D., et al. Drugging K-Ras(G12C) through covalent inhibitors: mission possible? LID - S0163-7258(19)30116-0 [pii] LID - 10.1016/j.pharmthera.2019.06.007 [doi].
- [33] Wiesweg M et al. Impact of RAS mutation subtype on clinical outcome—a cross-entity comparison of patients with advanced non-small cell lung cancer and colorectal cancer. *Oncogene* 2019;38:2953–66. <https://doi.org/10.1038/s41388-018-0634-0>.
- [34] De Rook W et al. Association of KRAS p. G13D mutation with outcome in patients with chemotherapy-refractory metastatic colorectal cancer treated With cetuximab. *JAMA* 2010;304:1812–20. <https://doi.org/10.1001/jama.2010.1535>.
- [35] Tural D, Fau - Selcukbiricik F, et al. Association KRAS G13D tumor mutated outcome in patients with chemotherapy refractory metastatic colorectal cancer treated with cetuximab.
- [36] Stolze B, Reinhart S, Bullinger L, Fröhling S, Scholl C. Comparative analysis of KRAS codon 12, 13, 18, 61, and 117 mutations using human MCF10A isogenic cell lines. *Sci Rep* 2015;5:8535. <https://doi.org/10.1038/srep08535>.
- [37] Hunter JC et al. Biochemical and structural analysis of common cancer-associated KRAS mutations. *Mol Cancer Res* 2015;13:1325. <https://doi.org/10.1158/1541-7786.MCR-15-0203>.
- [38] Smith MJ, Ikura M. Integrated RAS signaling defined by parallel NMR detection of effectors and regulators. *Nat Chem Biol* 2014;10:223. <https://doi.org/10.1038/nchembio.1435>.
- [39] Loree JM et al. Not all RAS mutations created equal: functional and clinical characterization of 80 different KRAS and NRAS mutations. *J Clin Oncol* 2017;35:3589. [https://doi.org/10.1200/JCO.2017.35.15\\_suppl.3589](https://doi.org/10.1200/JCO.2017.35.15_suppl.3589).
- [40] Munoz-Maldonado C, Zimmer Y, Medova M. A comparative analysis of individual RAS mutations in cancer biology. *Front Oncol* 2019;9:1088. <https://doi.org/10.3389/fonc.2019.01088>.
- [41] De Vivo M, Masetti M, Bottegoni G, Cavalli A. Role of molecular dynamics and related methods in drug discovery. *J Med Chem* 2016;59:4035–61. <https://doi.org/10.1021/acs.jmedchem.5b01684>.
- [42] Gorfe AA, Grant BJ, McCammon JA. Mapping the nucleotide and isoform-dependent structural and dynamical features of Ras proteins. *Structure* 2008;16:885–96. <https://doi.org/10.1016/j.str.2008.03.009>.
- [43] Prakash P et al. Dynamics of membrane-bound G12V-KRAS from simulations and single-molecule FRET in native nanodiscs. *Biophys J* 2019;116:179–83. <https://doi.org/10.1016/j.bpj.2018.12.011>.
- [44] Cao S et al. K-Ras G-domain binding with signaling lipid phosphatidylinositol (4,5)-phosphate (PIP2): membrane association, protein orientation, and function. *J Biol Chem* 2019;294:7068–84. <https://doi.org/10.1074/jbc.RA118.004021>.
- [45] Yu M, Chen Y, Wang Z-L, Liu Z. Fluctuation correlations as major determinants of structure- and dynamics-driven allosteric effects. *PCCP* 2019;21:5200–14. <https://doi.org/10.1039/C8CP07859A>.
- [46] Phillips JC et al. Scalable molecular dynamics with NAMD. *J Comput Chem* 2005;26:1781–802. <https://doi.org/10.1002/jcc.20289>.
- [47] Hornak V et al. Comparison of multiple amber force fields and development of improved protein backbone parameters. *Proteins-Struct Funct Bioinform* 2006;65:712–25. <https://doi.org/10.1002/prot.21123>.
- [48] Wang JM, Wolf RM, Caldwell JW, Kollman PA, Case DA. Development and testing of a general amber force field. *J Comput Chem* 2004;25:1157–74. <https://doi.org/10.1002/jcc.20035>.
- [49] Vatansever S, Gümüş ZH, Erman B. Intrinsic K-Ras dynamics: a novel molecular dynamics data analysis method shows causality between residue pair motions. *Sci Rep* 2016;6:37012. <https://doi.org/10.1038/srep37012>.
- [50] Humphrey W, Dalke A, Schulten K. VMD: Visual molecular dynamics. *J Mol Graph Model* 1996;14:33–8. [https://doi.org/10.1016/0263-7855\(96\)00018-5](https://doi.org/10.1016/0263-7855(96)00018-5).
- [51] Buhman Greg et al. Allosteric modulation of Ras positions Q61 for a direct role in catalysis. *Proceedings of the National Academy of Sciences* 2010;107(11):4931–6. <https://doi.org/10.1073/pnas.0912226107>.